The effects of interdiffusion on the subbands in $Ga_xIn_{1-x}N_{0.04}As_{0.96}$/GaAs quantum well for 1.3 and 1.55 μm operation wavelengths

Michael C. Y. Chan, Charles Surya,[a] and P. K. A. Wai
Department of Electronic and Information Engineering, The Hong Kong Polytechnic University, Hung Hom, Kowloon, Hong Kong

(Received 21 November 2000; accepted for publication 12 March 2001)

The interdiffusion of $Ga_xIn_{1-x}N_{0.04}As_{0.96}$/GaAs single quantum well (QW) structure with well width of 6 nm is studied theoretically. The as-grown Ga concentration in the QW is chosen to be 0.7 and 0.6 for the operation wavelengths of 1.3 and 1.55 μm, respectively. We studied the effects of interdiffusion on the in-plane strain, confinement potential, and subband energy levels of the QW using Fick's law. The diffusion coefficients of both the well and barrier layers are assumed to be constant. The effects of valence band mixing and strains are included in the calculation of the electron and hole subband structures. We find that the group-III interdiffusion effects can result in blueshifts of 123 and 211 nm in the $Ga_xIn_{1-x}N_{0.04}As_{0.96}$/GaAs QW at operation wavelength of 1.3 μm ($x=0.7$) and 1.55 μm ($x=0.6$), respectively. Our results show that interdiffusion technique can be used to tune the operating wavelengths of GaInAsN/GaAs lasers for multiwavelength applications such as in the sources of dense wavelength division multiplexed optical communication systems. © *2001 American Institute of Physics.* [DOI: 10.1063/1.1370110]

I. INTRODUCTION

Recently, GaInNAs has been grown pseudomorphically on GaAs substrates.[1] The incorporation of the smaller nitrogen atoms into the GaInAs layers reduces the net strain in the lattice and enables fabrication of long-wavelength optical devices such as high-performance laser diodes emitting at 1.3–1.55 μm for optical fiber communications.[1–11] Compared to GaInAsP quantum well (QW) systems,[11] GaInAsN/GaAs heterojunctions have larger conduction band offsets which lead to stronger electron confinement. The high-temperature performance of both edge-type and surface-type emitting GaInAsN/GaAs laser diodes[12] are expected to be better than that of GaInAsP devices.

One of the major research areas for bulk and QW semiconductor devices is to improve the performance and characteristics of optical devices by modification of band structures.[13–16] For QW devices, both the quantum size effect and the strain induced in the layered structure can be utilized to custom design the band structure such that laser diodes with high differential gain, low threshold current, high output power, and enhanced linewidth and modulation bandwidth are possible.[17–19]

Interdiffusion is a thermal process that facilitates the movement of constituent atoms across the heterointerface. Such movement will change both the band structure and optical properties of a QW. The major advantage of interdiffusion as a band-structure-engineering technique is the high accuracy in the tuning of the emission wavelength. Such fine tuning is necessary for application in standard dense wavelength division multiplexed optical communication systems, which has a wavelength grid of 100 GHz spacing as defined by International Telecommunication Union.

In this article, we present a detailed theoretical analysis of the interdiffused GaInAsN/GaAs QW on GaAs substrate. We focus on operation wavelengths of 1.3 and 1.55 μm because of their importance in optical fiber communications. In Sec. II, we will discuss the interdiffusion model and analyze the effects of strain in the QW structure. In Sec. III, we give the results of subband energy levels, in-plane strain, and optical transition energy as a function of the diffusion length. Finally, the conclusion is presented in Sec. IV

II. THEORETICAL MODEL

A. Diffusion model

We assume that Fick's second law applies in the QW layers and all atomic movements across the heterojunctions have the same diffusion coefficient. We further assume that the diffusion is contributed mainly by group-III sublattice diffusion, i.e., In and Ga atoms. Group-V sublattice diffusion is small because of the strong bond strength of N–As. The diffusion of In and Ga are assumed to be isotropic and the diffusion coefficient is independent of the concentration of In and Ga. The composition profile after interdiffusion is characterized by a diffusion length $L_d=\sqrt{(Dt)}$, where D is the diffusion coefficient and t is the annealing time. For a single GaInNAs/GaAs QW with the as-grown In mole fraction given by x_0, the composition profile of In after interdiffusion is given by

$$x(z)=\frac{x_0}{2}\left[\mathrm{erf}\left(\frac{L_z+2z}{4L_d}\right)+\mathrm{erf}\left(\frac{L_z-2z}{4L_d}\right)\right], \tag{1}$$

where L_z is the as-grown well width, z denotes the length along the crystal growth direction, and the QW is centered at $z=0$.

[a]Electronic mail: ensurya@polyu.edu.hk

0021-8979/2001/90(1)/197/5/$18.00 © 2001 American Institute of Physics

Downloaded 07 Apr 2011 to 158.132.161.9. Redistribution subject to AIP license or copyright; see http://jap.aip.org/about/rights_and_permissions

B. Effects of strain

Despite the lattice mismatch between the thin well and thick barrier QW material, the QW is pseudomorphic and has a uniform lattice constant throughout the whole structure. The mismatch does result in tetragonal deformation of the lattice and manifests as strain perpendicular to the heterointerface. If the growth direction z is along ⟨001⟩, the GaInAsN well layer is subjected to biaxial compressive in-plane strains parallel to the x direction along ⟨100⟩ and to y direction along ⟨010⟩. There is also a uniaxial shear strain parallel to the z direction along ⟨001⟩. The in-plane strain across the well will vary according to the composition of the alloy concentration after interdiffusion. The biaxial in-plane strains and uniaxial shear strain after interdiffusion are given by[20,21]

$$\epsilon_{xx}=\epsilon_{yy}=\epsilon(x), \tag{2a}$$

$$\epsilon_{zz}=-2[c_{12}(x)/c_{11}(x)]\epsilon(x), \tag{2b}$$

$$\epsilon_{xx}=\epsilon_{yy}=\epsilon(x), \tag{2c}$$

where $\epsilon(x)$ is the misfit factor between the well and the barrier, which is negative for compressive strain. The parameters $c_{11}(x)$ and $c_{12}(x)$ are the elastic stiffness constants. The change in the bulk band gap, $S_{\perp}(x)$, as a result of the hydrostatic strain, is given by

$$S_{\perp}(x)=-2a(x)[1-c_{12}(x)/c_{11}(x)]\epsilon(x). \tag{3}$$

The hydrostatic deformation potential $a(x)$ is calculated from

$$a(x)=-\frac{1}{3}[c_{11}(x)+2c_{12}(x)]\frac{dE_g}{dP}, \tag{4}$$

where dE_g/dP is the hydrostatic pressure coefficient of the lowest direct energy gap E_g. The splitting energy, $S_{\parallel}(x)$, between the heavy hole (HH) and light hole (LH) band edges induced by the shear component of the strain is

$$S_{\parallel}(x)=-b(x)[1+2c_{12}(x)/c_{11}(x)]\epsilon(x), \tag{5}$$

where $b(x)$ is the shear deformation potential. The coupling between the LH and split-off band results in asymmetric heavy hole to light hole splitting. We have

$$S_{\parallel \mathrm{HH}}(x)=S_{\parallel}(x), \tag{6}$$

$$S_{\parallel \mathrm{LH}}(x)=-\tfrac{1}{2}[S_{\parallel}(x)+\Delta_0(x)]+\tfrac{1}{2}[9S_{\parallel}(x)+\Delta_0(x)^2-2S_{\parallel}(x)\Delta_0(x)]^{1/2}, \tag{7}$$

where $\Delta_0(x)$ is the spin-orbit splitting. The QW confinement potential $U_r(x)$, after the intermixing process is obtained by modifying the unstrained potential profile $\Delta E_r(x)$ with the variable strain effects. The QW confinement potential is given by

$$U_r(x)=\Delta E_r(x)-S_{\perp r}(x)\pm S_{\parallel r}(x), \tag{8}$$

where $S_{\perp r}(x)=Q_r S_{\perp}(x)$. The "+" and "−" signs represent the confined HH and LH profiles, respectively, and $S_{\parallel c}(x)=0$.

C. Subband energy

We apply the multiband effective mass theory in the envelope function scheme to calculate the electron and hole wave functions in the QW. For most III–V semiconductors, such as GaAs-based materials, the conduction and valence bands are decoupled. The wave functions of the electron and hole subband edge at the zone center of Γ_6 valley symmetry can be calculated separately in accordance to the Ben–Daniel and Duke model.[22] The wave equation has the form of a one-dimensional Schrödinger-like equation as given below

$$-\frac{\hbar^2}{2}\frac{d}{dz}\left[\frac{1}{m_r^*(z)}\frac{d\psi_{rl}(z)}{dz}\right]+U_r(z)\cdot\psi_{rl}(z)=E_{rl}\psi_{rl}(z), \tag{9}$$

where $\psi_{rl}(z)$ is the wave function of the lth subband for electrons ($r=e$), heavy hole ($r=$HH) or light holes ($r=$LH), respectively, $m_r^*(z)$ is the corresponding carrier effective mass in the z direction, E_{rl} is the subband-edge energy. Equation (9) is solved numerically using a finite difference method with the confinement profile given in Eq. (8).

TABLE I. The room temperature material parameters of GaAs, GaN, InAs, and InN used in the numerical calculations.

	GaAs[a]	GaN[b]	InAs[a]	InN	Units
a_0	5.6533	4.46	6.0583	5.02[c]	Å
c_{11}	11.9	29.6	8.329	18.4[d]	$\times 10^{11}$ dyn/cm^2
c_{12}	5.38	15.4	4.526	11.6[d]	$\times 10^{11}$ dyn/cm^2
dE_g/dP	11.3	32.0	10.2	22.0[e]	$\times 10^{-6}$ eV/bar
b	−1.7	−2.67	−1.8	−2.67[b]	eV
m_c	0.0632	0.13	0.0213	0.14[f]	M_0
m_{HH}	0.5	0.806	0.517	0.8[f]	M_0
m_{LH}	0.088	0.205	0.024	0.19[f]	M_0
Δ_0	0.34	0.011	0.41	0.006[f]	eV
E_g	1.424	3.1	0.354	1.9[g]	eV

[a]Reference 24.
[b]Reference 26.
[c]Reference 27.
[d]Reference 28.
[e]Reference 29.
[f]Reference 30.
[g]Reference 31.

Downloaded 07 Apr 2011 to 158.132.161.9. Redistribution subject to AIP license or copyright; see http://jap.aip.org/about/rights_and_permissions

TABLE II. The bowing factors used in calculations.

$C_{\text{In-Ga}}$(InGaN)	$C_{\text{In-Ga}}$(InGaAs)	$C_{\text{As-N}}$(InNAs)	$C_{\text{As-N}}$(GaNAs)
1.4 eV[a]	0.51 eV[b]	4.22 eV[c]	20 eV[d]

[a]Reference 32.
[b]Reference 24.
[c]Reference 33.
[d]Reference 34.

III. RESULTS AND DISCUSSION

We study a QW layer with a 6 nm thick $Ga_xIn_{1-x}N_{0.04}As_{0.96}$ well sandwiched between a 20 nm thick GaAs barrier theoretically. We assumed that the envelope functions satisfy the boundary conditions at the interface. It has been shown that results from effective mass theory agree with experimental measurements down to a well width of 2 nm for GaAs-based QW.[23] The error due to the effective mass approximation for a 6 nm thick well should therefore be negligible. Since the QW is strained at about 2% only for an In composition equal to or less than 0.4, the 6 nm well width we chose is below the critical thickness for the formation of misfit dislocations. In our calculation, the as-grown Ga concentration in the QWs are set to be 0.7 and 0.6 corresponding to emission wavelengths of 1.3 and 1.55 μm, respectively. The subband energies at the band edge of QW are calculated using Eqs. (1)–(9). The material parameters of GaAs, GaN, InAs, and InN at room temperature are given in Table I. Most of the values are determined by interpolation of the binary parameters at 300 K by Vegard's Law. The generalized parameter T for the quaternary material $A_xB_{1-x}C_yD_{1-y}$, is derived from the parameters of the four binary compounds AC, AD, BC, and BD, i.e.,

$$T(x,y)=(1-x)yT_{BC}+xyT_{AC}+x(1-y)T_{AD}+(1-x)(1-y)T_{BD}. \quad (10)$$

The bulk band gap of $Ga_xIn_{1-x}N_yAs_{1-y}$ compositional dependence, in eV, is calculated using[24]

$$\begin{aligned}E_g(x,y)=&xyE_g(\text{GaN})+(1-x)yE_g(\text{InN})+x(1-y)\\&\times E_g(\text{GaAs})+(1-x)(1-y)E_g(\text{InAs})+x(x-1)\\&\times[yC_{\text{In-Ga}}(\text{InGaN})+(1-y)C_{\text{In-Ga}}(\text{InGaAs})]\\&+y(y-1)[xC_{\text{As-N}}(\text{InNAs})\\&+(1-x)C_{\text{As-N}}(\text{GaNAs})],\end{aligned} \quad (11)$$

where, for example, $C_{\text{In-Ga}}$(InGaN) is the band gap nonlinearity factor (bowing factor) of InGaN. All the relevant bowing factors are listed in Table II. The partition ratio for the band edge discontinuity at the heterojunction of the valence and conduction bands is taken to be 20:80 (i.e., $Q_c=0.8$) from experimental measurements.[2] Khreis *et al.*[25] reported that the diffusion length of In–Ga interdiffusion in the InGaAs/GaAs QW system with an annealing temperature of 850 °C and an annealing time of 6 min is 1.0–2.0 nm.[24]

The modification of transition energy is due to the change of compositional alloys, the in-plane strain, and the subband energy of the GaInNAs/GaAs QW. In the group-III interdiffusion, In atoms diffuse into the GaAs barrier layer and Ga atoms diffuse into the well layer. A thin and graded GaInNAs/InGaAs interface is formed. The distribution of the In and Ga atoms are described by the error function distribution, while the As and N concentration profiles do not change. The Ga profiles of the as-grown and interdiffused $Ga_{0.7}In_{0.3}N_{0.04}As_{0.96}$/GaAs QW are shown in Fig. 1. Initially, the diffusion length is small. The Ga atoms near the interface diffuse into the well, while In atoms diffuse into the barrier, but there is little change in the Ga concentration at the central well region. As the interdiffusion process proceeds, the Ga concentration at the central well region changes from 70% to 75% as the diffusion length increases from 0 to 1.5 nm. The as-grown square well structure gradually changes from an abrupt interface to a graded profile as a result of the interdiffusion of atoms. Other material parameters, such as band gap energy, will also be modified. In the case of $Ga_{0.6}In_{0.4}N_{0.04}As_{0.96}$/GaAs QW interdiffusion, the shapes of the Ga profile are very similar to that of a $Ga_{0.7}In_{0.3}N_{0.04}As_{0.96}$/GaAs QW, and are therefore not shown. The concentration of Ga at the central well region changes from 60% to 66.3% as the diffusion length increases from 0 to 1.5 nm.

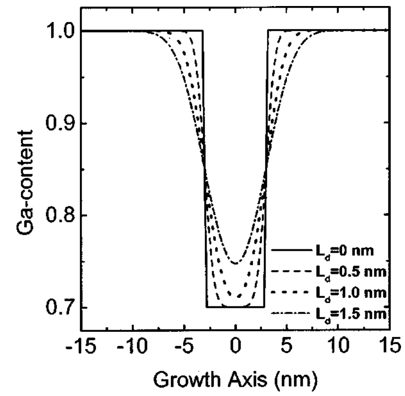

FIG. 1. Ga compositional profiles of $Ga_{0.7}In_{0.3}N_{0.04}As_{0.96}$/GaAs QW for different diffusion lengths. The as-grown well width is 6.0 nm.

Interdiffusion modifies the composition, which in turn changes the in-plane strain. The variations of the in-plane strain profiles for the $Ga_{0.7}In_{0.3}N_{0.04}As_{0.96}$/GaAs QW as the diffusion length changes are shown in Fig. 2. The diffusion

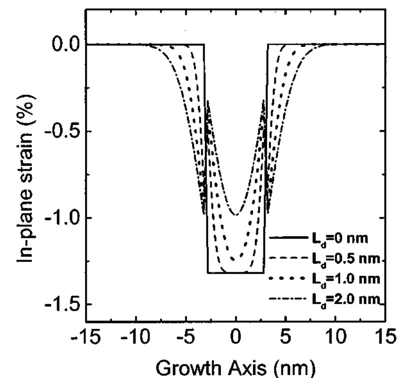

FIG. 2. In-plane strain across the $Ga_{0.7}In_{0.3}N_{0.04}As_{0.96}$/GaAs interdiffused QW for various diffusion length.

Downloaded 07 Apr 2011 to 158.132.161.9. Redistribution subject to AIP license or copyright; see http://jap.aip.org/about/rights_and_permissions

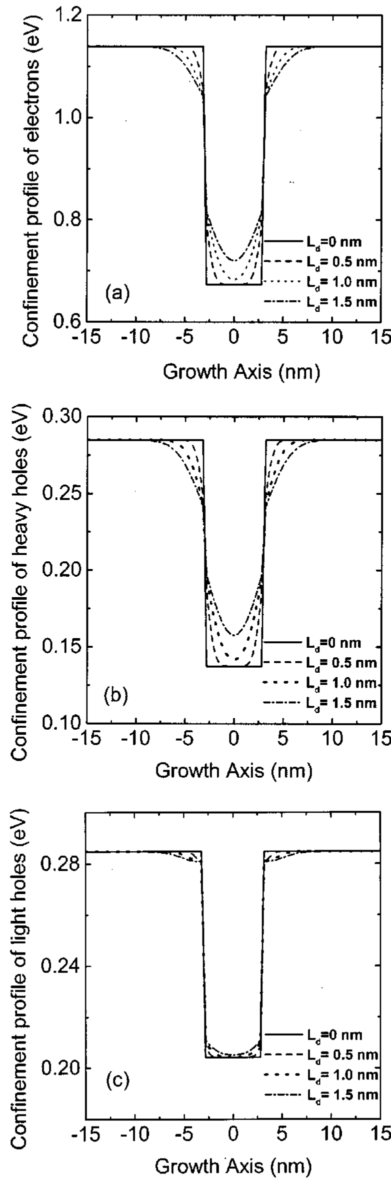

FIG. 3. The confinement profiles of (a) electrons in the conduction band, (b) heavy holes, and (c) light holes in valence band across the $Ga_{0.7}In_{0.3}N_{0.04}As_{0.96}$/GaAs interdiffused QW for different diffusion lengths.

of In atoms into the barrier layer reduces the lattice misfit at the heterointerface. In other words, the interdiffusion process results in strain relaxation in the well layer. For the as-grown QW, the strain is 1.3% and 2.0% at the central well region for the $Ga_{0.7}In_{0.3}N_{0.04}As_{0.96}$ and $Ga_{0.6}In_{0.4}N_{0.04}As_{0.96}$ well layers, respectively. The interdiffusion process reduces the compressive strain to a mere 0.98% and 1.58% for the $Ga_{0.7}In_{0.3}N_{0.04}As_{0.96}$ and $Ga_{0.6}In_{0.4}N_{0.04}As_{0.96}$ well layers, respectively. At the barrier regions, the compressive strain increases as the In concentration increases near the interface. The compressive strain reaches up to 1.0% and 1.2% for the $Ga_{0.7}In_{0.3}N_{0.04}As_{0.96}$ and $Ga_{0.6}In_{0.4}N_{0.04}As_{0.96}$ well layers at the diffusion length $L_d = 1.5$ nm, respectively.

Figures 3(a)–3(c) show the confinement profiles of the electrons in the conduction band, heavy holes, and light holes in the valence bands for the as-grown and interdiffused $Ga_{0.7}In_{0.3}N_{0.04}As_{0.96}$/GaAs QW with different diffusion lengths. The shapes of the confinement profiles are determined by the variation of bulk material band gap energy and the in-plane strain. The effective barrier heights (band gap discontinuity) are due to the high Ga concentration in $Ga_xIn_{1-x}N_{0.04}As_{0.96}$ alloys. We observe that the effective barrier heights of all confinement profiles, except for the light hole in the valence band, are reduced. The conduction band offset (see Table III) is reduced from 466.6 to 419.2 meV when the diffusion length changes from 0 to 1.5 nm. We note that this offset remains large after the QW interdiffusion. The large offset results in better confinement of electrons at high temperatures, which lead to better high temperature characteristics for long wavelength laser diodes. Interdiffusion also enlarges the effective well width at the top and reduces that at the bottom of the well. The potential energy profile of the light hole in the valence band for the interdiffused QW structure remains abrupt. The well width which equals that of the as-grown QW. Similar properties are also observed in the $Ga_{0.6}In_{0.4}N_{0.04}As_{0.96}$/GaAs QW interdiffusion. Corresponding figures are therefore not shown here.

The variations of bulk band gap energy of $Ga_{1-x}In_xN_{0.04}As_{0.96}$ in the central well region are given in Table III. Due to the effects of strain, the transition energies are affected by the change of the hydrostatic and shear de-

TABLE III. The changes in bulk band gap, hydrostatic deformation, shear deformation potential energy, and conduction band offset versus diffusion lengths.

L_d (nm)	0	0.5	1.0	1.5
$Ga_{0.7}In_{0.3}N_{0.04}As_{0.96}$/GaAs				
bulk band gap (eV)	0.710	0.710	0.729	0.801
hydrostatic deformation potential (eV)	0.131	0.131	0.124	0.099
shear deformation potential of HH (eV)	0.031	0.031	0.029	0.022
shear deformation potential of LH (eV)	0.036	0.036	0.034	0.025
conduction band offset (meV)	466.6	466.6	456.4	419.2
$Ga_{0.6}In_{0.4}N_{0.04}As_{0.96}$/GaAs				
bulk band gap (eV)	0.526	0.526	0.550	0.640
hydrostatic deformation potential (eV)	0.193	0.193	0.185	0.155
shear deformation potential of HH (eV)	0.051	0.051	0.048	0.038
shear deformation potential of LH (eV)	0.063	0.063	0.048	0.038
conduction band offset (meV)	564.2	564.2	551.2	503.0

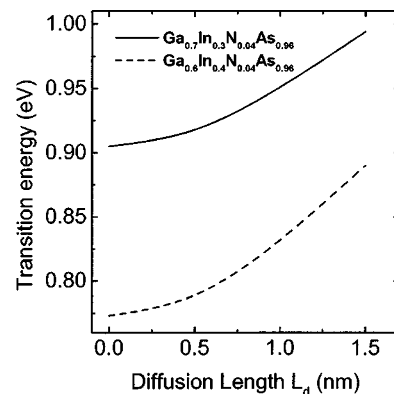

FIG. 4. The transition energy of $Ga_xIn_{1-x}N_{0.04}As_{0.96}$/GaAs interdiffused QW as a function of L_d.

Downloaded 07 Apr 2011 to 158.132.161.9. Redistribution subject to AIP license or copyright; see http://jap.aip.org/about/rights_and_permissions

formation potential energies. It is worth noticing that at the initial stage of interdiffusion when L_d is smaller than 0.5 nm, the hydrostatic and shear deformation potential energies do not change. The results also show that the changes of bulk band gap energy are the main contribution to the shift in transition energy. Finally, the variations of transition energy of interdiffused $Ga_xIn_{1-x}N_{0.04}As_{0.96}$/GaAs QW with $x=0.7$ and 0.6 against diffusion lengths are shown in Fig. 4. Blueshifts of 89 and 117 meV are obtained for the $Ga_{0.7}In_{0.3}N_{0.04}As_{0.96}$ layer and $Ga_{0.6}In_{0.4}N_{0.04}As_{0.96}$ layer, respectively, as L_d varies from 0 to 1.5 nm.

IV. CONCLUSION

In conclusion, we have presented a theoretical study of the effects of group III interdiffusion on $Ga_xIn_{1-x}N_{0.04}As_{0.96}$/GaAs QW. The well width is 6.0 nm. We chose the as-grown Ga concentration in the QW to be 0.7 and 0.6, which correspond to operation wavelengths of 1.3 and 1.55 μm, respectively. We used Fick's law with constant diffusion coefficients for both the well and barrier layers. Group-V interdiffusion is neglected because of the strong bond strength of N–As. We use an error function distribution for the diffused compositional profile. We determined the optical transition energies after the QW interdiffusion. We calculated the electron and hole subband energies for different diffusion lengths of the QW interdiffusion process. We find that the blueshift of the operation wavelengths can be tuned from 0.905 (1.371 μm) to 0.994 eV (1.248 μm) and 0.773 (1.605 μm) to 0.89 eV (1.394 μm) in the $Ga_{0.7}In_{0.3}N_{0.04}As_{0.96}$ layer and $Ga_{0.6}In_{0.4}N_{0.04}As_{0.96}$ layer, respectively, if the diffusion lengths vary from 0 to 1.5 nm. The results demonstrated that the interdiffusion processes can be used to fine tune the operation wavelengths at 1.3 and 1.55 μm for applications in dense wavelength division multiplexed optical communication systems.

ACKNOWLEDGMENTS

The work described in this article was partially supported by a grant from the Research Grants Council of the Hong Kong Special Administrative Region, China (Project No. PolyU5138/97E). Additional support was provided by a grant from the University Research Grants of The Hong Kong Polytechnic University.

[1] M. Sopanen, H. P. Xin, and C. W. Tu, Appl. Phys. Lett. **76**, 994 (2000).
[2] M. Hetterich, M. D. Dawson, A. Yu. Egorov, D. Bernklau, and H. Riechert, Appl. Phys. Lett. **76**, 1030 (2000).
[3] N. Y. Li, C. P. Hains, K. Yang, J. Lu, J. Cheng, and P. W. Li, Appl. Phys. Lett. **75**, 1051 (1999).
[4] H. P. Xin, C. W. Tu, and M. Geva, Appl. Phys. Lett. **75**, 1416 (1999).
[5] H. P. Xin, K. L. Kavanagh, Z. Q. Zhu, and C. W. Tu, Appl. Phys. Lett. **74**, 2337 (1999).
[6] H. P. Xin and C. W. Tu, Appl. Phys. Lett. **72**, 2442 (1998).
[7] J. B. Heroux, X. Yang, and W. I. Wang, Appl. Phys. Lett. **75**, 2716 (1999).
[8] Z. Pan, T. Miyamoto, D. Schlenker, S. Sato, F. Koyama, and K. Iga, J. Appl. Phys. **84**, 6409 (1998).
[9] T. Kageyama, T. Miyamoto, S. Makino, F. Koyama, and K. Iga, Jpn. J. Appl. Phys., Part 2 **38**, L298 (1999).
[10] T. Kitatani, K. Nakahara, M. Kondow, K. Uomi, and T. Tanaka, J. Cryst. Growth **209**, 345 (2000).
[11] M. Kondow, K. Uomi, A. Niwa, T. Kitatani, S. Watahiki, and Y. Yazawa, Jpn. J. Appl. Phys., Part 1 **35**, 1273 (1996).
[12] M. Kondow, S. Nakatsuka, T. Kitatani, Y. Yazawa, and M. Okai, Jpn. J. Appl. Phys., Part 1 **35**, 5711 (1996).
[13] M. C. Y. Chan, E. M. T. Cheung, and E. H. Li, Mater. Sci. Eng., B **B59**, 283 (1999).
[14] M. C. Y. Chan, P. C. K. Kwok, and E. H. Li, IEEE J. Sel. Top. Quantum Electron. **4**, 685 (1998).
[15] M. C. Y. Chan, E. H. Li, and K. S. Chan, Phys. B **245**, 317 (1998).
[16] M. C. Y. Chan, Y. Chan, and E. H. Li, IEEE J. Quantum Electron. **34**, 519 (1998).
[17] F. Agahi, K. M. Lau, H. K. Choi, A. Baliga, and N. G. Anderson, IEEE Photonics Tech. Lett. **7**, 140 (1995).
[18] J. Werner, E. Kapon, N. G. Stoffel, E. Colas, S. A. Schwarz, C. L. Schwartz, and N. Andreadakis, Appl. Phys. Lett. **55**, 540 (1989).
[19] H. Ribot, K. W. Lee, R. J. Simes, R. H. Yan, and L. A. Coldren, Appl. Phys. Lett. **55**, 672 (1989).
[20] D. Ahn and S. L. Chuang, IEEE J. Quantum Electron. **24**, 2400 (1988).
[21] S. L. Chuang, Phys. Rev. B **43**, 9649 (1991).
[22] D. J. Ben-Daniel and C. B. Duke, Phys. Rev. **152**, 638 (1966).
[23] K. J. Moore, G. Duggan, P. Dawson, and C. T. Foxon, Phys. Rev. B **38**, 5535 (1988).
[24] E. H. Li, Phys. E (Amsterdam) **5**, 215 (1999).
[25] O. M. Khreis, K. P. Homewood, and W. P. Gillin, J. Appl. Phys. **84**, 232 (1998).
[26] S. H. Park and S. L. Chuang, J. Appl. Phys. **87**, 353 (2000).
[27] S. Strite, D. Chandrasekhar, D. J. Smith, J. Sariel, H. Chen, N. Teraguchi, and H. Morkoc, J. Cryst. Growth **127**, 204 (1993).
[28] A. F. Wright, J. Appl. Phys. **82**, 2833 (1997).
[29] K. Kim, W. R. L. Lambrecht, and B. Segall, Phys. Rev. B **53**, 16310 (1996).
[30] A. T. Meney, E. P. O'Reilly, and A. R. Adams, Semicond. Sci. Technol. **11**, 897 (1996).
[31] V. I. Gavrilenko and R. Q. Wu, Phys. Rev. B **61**, 2632 (2000).
[32] R. Goldhahn, J. Scheiner, S. Shokhovets, T. Frey, U. Kohler, D. J. As, and K. Lischka, Appl. Phys. Lett. **76**, 291 (2000).
[33] T. Yang, S. Nakajima, and S. Sakai, Jpn. J. Appl. Phys., Part 2 **36**, L320 (1997).
[34] M. Kondow, K. Uomi, K. Hosomi, and T. Mozume, Jpn. J. Appl. Phys., Part 2 **33**, L1056 (1992).

Downloaded 07 Apr 2011 to 158.132.161.9. Redistribution subject to AIP license or copyright; see http://jap.aip.org/about/rights_and_permissions